JGR Oceans

RESEARCH ARTICLE
10.1029/2022JC019126

Restratification Structure and Processes in the Irminger Sea

M. F. Sterl[1,2] **and M. F. de Jong**[1]

[1]Department of Ocean Systems, NIOZ, Royal Netherlands Institute for Sea Research, Texel, The Netherlands, [2]Institute for Marine and Atmospheric Research, Utrecht University, Utrecht, The Netherlands

Key Points:

- Restratification in the Irminger Sea is distinctly different in the upper 100 m of the water column than below
- In the upper layer, summers with exceptionally high stratification had strong atmospheric heat and freshwater gain
- In the lower layer, restratification is driven by lateral advection of warm and saline waters through Irminger Current eddies

Supporting Information:

Supporting Information may be found in the online version of this article.

Correspondence to:

M. F. Sterl,
miriam.sterl@nioz.nl

Citation:

Sterl, M. F., & de Jong, M. F. (2022). Restratification structure and processes in the Irminger Sea. *Journal of Geophysical Research: Oceans*, *127*, e2022JC019126. https://doi.org/10.1029/2022JC019126

Received 25 JUL 2022
Accepted 13 DEC 2022

Abstract The Irminger Sea is one of the few regions in the ocean where deep (>1,000 m) convection occurs. Convection is followed by restratification during summer, when the stratification of the water column is reestablished and the convectively formed water is exported at depth. There are currently no descriptions of interannual variability and physical drivers of restratification in the Irminger Sea. We investigate restratification in the upper 600 m of the central Irminger Sea using reanalysis data for the years 1993–2019. We find distinctly different restratification processes in the upper 100 m (the upper layer) and the water below it (the lower layer). In the upper layer, the stratification is dominated by a seasonal cycle that matches the cycle of the surface heat flux. In 2010 and 2019, there were peaks in upper layer restratification, which could partly be related to strong atmospheric heat and freshwater fluxes. Greenland runoff likely also contributed to the high restratification, although this contribution could not be quantified in the present study. In the lower layer there is strong interannual variability in stratification, caused by variability both in the convection and the restratification strength. The restratification strength is strongly correlated with the eddy kinetic energy in the eastern Irminger Sea, suggesting that lower layer restratification is driven by lateral advection of warm, saline waters through Irminger Current eddies. In the future, surface warming and freshening of the Irminger Sea due to anthropogenic climate change are expected to increase upper layer stratification, potentially inhibiting convection.

Plain Language Summary In the Irminger Sea, cold winters can cause the ocean's surface waters to cool enough that they start mixing downward. The mixing can continue for months and eventually form a dense water mass of more than 1 km deep. This process is called deep convection. During summer, the dense water gets exported at depth, and the water column will go back to its original structure with lighter waters over denser waters. This is called restratification. The formation and export of dense waters in the Irminger Sea plays an important role in the global ocean circulation. Here we study what drives the restratification in the Irminger Sea, and how it varies in time. We find that in the upper 100 m the restratification is influenced by heating from the atmosphere, which warms the surface waters and makes them lighter. Additionally, rainfall or ice melt which make the surface waters fresher can contribute to restratification. Below the surface layer, restratification happens through transport of warm and saline waters from the eastern Irminger Sea. With rising ocean temperatures due to climate change, the Irminger Sea might see more restratification in the future, which might slow down global oceanic heat transport.

1. Introduction

The Atlantic Meridional Overturning Circulation (AMOC) plays an important role in the global climate system (e.g., Fox-Kemper et al., 2021; McCarthy et al., 2017; Pérez et al., 2013). In the Atlantic upper ocean, warm and saline waters are transported northward in the AMOC's upper limb from the equator to high latitudes, where they are transformed into colder and denser waters. These dense waters can spread to the AMOC's lower limb in the deep ocean, where they remain isolated from the atmosphere for hundreds of years (England, 1995). Thus the AMOC has an important effect on the ocean's uptake and storage of heat and anthropogenic CO_2 from the atmosphere (Brown et al., 2021; Fröb et al., 2016). One of the processes that adds to the water mass transformation at high latitudes is deep convection. Deep convection can theoretically be described as a three-phase process (de Jong et al., 2018; Gelderloos et al., 2011; Jones & Marshall, 1997; Marshall & Schott, 1999). It starts with the preconditioning phase, which consists of a large-scale (order of 100 km) cyclonic gyre circulation with "doming" isopycnals, bringing weakly stratified waters of the interior close to the surface. The second phase is the deep convection phase, during which strong winter buoyancy loss gradually deepens the mixed layer, forming a large and deep "mixed patch" or "convective patch" with a diameter in the order of 100 km and a depth in the

order of 1 km. The deep convection is followed by the restratification phase which occurs after winter, in spring and summer, on a time scale of weeks to months. During this phase the stratification of the convective patch is reestablished by surface buoyancy gain and by lateral exchange between the convective patch and its stratified environment. The restratification determines the stratification at the start of the next deep convection phase and thus affects preconditioning. There are only a few areas in the world's oceans where deep convection (more than 1 km) occurs. Two important deep convection regions are the Labrador Sea (e.g., Lazier et al., 2002; Lilly et al., 1999; Straneo, 2006a; Yashayaev & Loder, 2017) and the Irminger Sea (e.g., de Jong & de Steur, 2016; de Jong et al., 2012, 2018; Pickart et al., 2003; Piron et al., 2016), located west and east of Greenland, respectively. The convectively formed dense waters in these basins can spread to the seas' perimeter and enter the lower limb of the AMOC (Georgiou et al., 2019; Katsman et al., 2018; Le Bras et al., 2020; Straneo, 2006b).

Multiple studies have addressed the restratification phase in the Labrador Sea. It was found that there is interannual variability in the deep convection as well as in the restratification in the Labrador Sea (e.g., de Jong et al., 2016; Lazier et al., 2002; Straneo, 2006a). Straneo (2006a) found that there are distinct temporal behaviors in the surface layer between 0 and 200 m and the lower layer between 200 and 1,300 m in the Labrador Sea interior. The surface layer properties follow a strong seasonal cycle, whereas the lower layer properties show strong interannual variability. Moreover, the surface layer freshens during summer and becomes more saline during winter; these signs in the seasonal cycle are reversed for the lower layer. Many studies have focused on the lateral exchange between the interior, where deep convection occurs, and the buoyant cyclonic boundary current in the Labrador Sea. Katsman et al. (2004) and Gelderloos et al. (2011) found that Irminger Rings (IRs) shed by the West Greenland Current (WGC) near the west coast of Greenland are an important contributor to restratification. Observations from Lilly et al. (1999), Hátún et al. (2007), and de Jong et al. (2014) show that IRs consist of a warm and saline core topped by a colder and fresher surface layer. This can be related to the structure of the WGC, which consists of warm and saline Irminger Sea Water below colder and fresher polar waters (Cuny et al., 2002). The IR vertical structure contributes to the distinct behaviors in the upper and lower layer in the interior Labrador Sea found by Straneo (2006a).

Deep convection also occurs in the cyclonic Irminger Gyre (de Jong & de Steur, 2016; de Jong et al., 2012, 2018; Våge et al., 2011). Recent studies by Lozier et al. (2019), Petit et al. (2020), and Li et al. (2021) found that deep convection in the Irminger Sea is a major contributor to overturning in the North Atlantic subpolar gyre. Moreover, the Irminger Sea is found to be an important region for anthropogenic carbon uptake (Fröb et al., 2016). While the relation between surface buoyancy forcing and Irminger Sea deep convection has been described (de Jong & de Steur, 2016; de Jong et al., 2012, 2018), the relation to changes in stratification is less explored. Since deep convection is predicted to weaken under climate change as a result of increasing stratification, it is important to study processes that contribute to stratification in the Irminger Sea. Therefore, this study aims to provide a description of the vertical structure and temporal variability of restratification in the Irminger Sea, as well as of the physical processes that contribute to it.

This paper is organized as follows: in Section 2, the data sets and methods used for the study are introduced. We employ an ocean reanalysis, validated against local mooring data, as well as surface flux data from atmospheric reanalysis. In Section 3, we describe the general hydrographic properties in the Irminger Sea and the interannual variability in stratification; moreover, we investigate the physical processes, such as surface forcing and eddy processes, that contribute to restratification. Finally, a summary and discussion of the results are presented in Section 4.

2. Data and Methods

2.1. Data

We used the GLORYS12V1 global ocean physics reanalysis from the Copernicus Marine Environment Monitoring Service (CMEMS; Drévillon et al., 2021) to investigate hydrographic variability in the Irminger Sea. GLORYS12V1 is an eddy-resolving reanalysis product. It uses the NEMO model component (Madec, 2016) and is forced at the surface by ECMWF ERA-Interim reanalysis from 1993 to 2017, which was replaced by ERA5 reanalysis for recent years. For this study, we used the monthly mean data for the period from January 1993 until December 2019. The data set has a spatial resolution of 1/12° and has 50 vertical levels, with vertical intervals in the order of 1 m in the upper 60 m, in the order of 10 m down to 550 m depth, and in the order 100 m down to

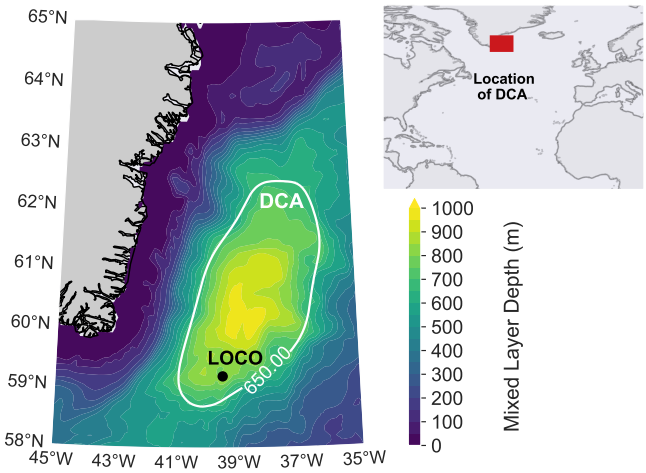

Figure 1. The mixed layer depth (MLD) field averaged over the months from the monthly 1993–2019 CMEMS data set in which the maximum MLD within the region [45°W, 35°W] × [58°N, 65°N] exceeds 1,000 m. In white, the 650 m contour of this MLD field smoothed with a Gaussian filter ($\sigma = 5$ grid cells) is shown, representing the boundary of the Deep Convection Area (DCA). The black dot shows the location of the LOCO mooring used for data validation. The panel in the upper right shows where the study area is located within the North Atlantic.

the bottom, increasing to 450 m in the deepest layer. The variables obtained from the data set are the potential temperature (`thetao`), practical salinity (`so`), eastward and northward ocean current velocity (`uo` and `vo`), and mixed layer depth (MLD) (`mlotst`). The MLD (henceforth abbreviated as MLD) in CMEMS is defined as the depth where the density difference compared to a reference level is 0.01 kg/m^3 (Madec, 2016, p. 246). The TEOS-10 software was used to recompute practical salinity to absolute salinity S_A, and potential temperature to conservative temperature Θ (McDougall & Barker, 2011). From these properties, the potential density anomaly referenced to the surface, σ_0, could then be computed. From now on, unless explicitly stated otherwise, every mention of salinity, temperature, and density from the CMEMS data will refer to S_A, Θ, and σ_0, respectively. The current velocities were used to compute eddy kinetic energy (EKE), defined as

$$\mathrm{EKE} = \frac{1}{2}\left[(u-\bar{u})^2 + (v-\bar{v})^2\right], \quad (1)$$

where $\bar{u}$ and $\bar{v}$ are the time-mean zonal and meridional velocity components over the whole time series.

To validate the CMEMS data, it was compared to data from the Long-term Ocean Circulation Observations (LOCO) mooring, which was located at 39.5°W, 59.2°N (Figure 1) from September 2003 until June 2018. The processed data from September 2003 until July 2015 as published by de Jong et al. (2012), de Jong and de Steur (2016), and de Jong et al. (2018) were used. The LOCO data is not assimilated in the CMEMS reanalysis and therefore provides an independent comparison of the reanalysis data with observations. For the comparison, the original daily resolution of the LOCO data was reduced to monthly means. This time series is compared to the CMEMS data interpolated at the LOCO mooring location. The comparison between the two data sets is described in Supporting Information S1.

To study atmospheric fluxes at the ocean surface, we used the ERA5 reanalysis from the Copernicus Climate Change Service (C3S) Climate Data Store (Hersbach et al., 2020). The monthly averaged data at the surface was selected for January 1993 until December 2019. The data set has a horizontal resolution of 0.25°. For freshwater fluxes the evaporation (`e`) and total precipitation (`tp`) were studied; the sum of these two yields the net atmospheric freshwater flux $\mathcal{F}$. For heat fluxes the surface net solar radiation (`ssr`), surface net thermal radiation (`str`), surface latent heat flux (`slhf`), and surface sensible heat flux (`sshf`) were used to obtain the net atmospheric heat flux Q.

2.2. Methods

2.2.1. Defining the Deep Convection Area

Because the aim of this study is to describe restratification after deep convection, we needed to identify the area within the Irminger Sea where deep convection occurs. We focused on the southwestern part of the Irminger Sea, where the center of the cyclonic Irminger Gyre is located. Out of the 27 years within the CMEMS data set, there are 28 months in which MLDs of more than 1 km deep occurred in this region. The MLD field was averaged over these months and the result is shown in Figure 1. The 650 m contour of this MLD field smoothed with a Gaussian filter ($\sigma = 5$ grid cells = 5/12°) was chosen as the boundary of the Deep Convection Area (DCA), which we will abbreviate as DCA. This particular contour was chosen because it contains the deep MLD centre, without extending so far northward that it contains part of the warm Irminger Current (IC), which should not be part of the cold convection region. The data from the CMEMS and ERA5 reanalyses were averaged over the DCA to get time series of surface freshwater and heat fluxes, MLD, and salinity, temperature and density profiles in the DCA.

2.2.2. Quantifying Stratification and Restratification

As a quantitative measure of the stratification of the part of the water column between $z = -h_1$ and $z = -h_2$ (where $0 \leq h_1 < h_2$), we used the stratification index (SI), defined as the integral of the potential density gradient times depth:

$$\mathrm{SI} = \int_{-h_2}^{-h_1} \frac{\partial \sigma}{\partial z} z \, \mathrm{d}z, \tag{2}$$

with units of kg/m^2. Partial integration of Equation 2 yields an expression of the SI in terms of the density profile $\sigma(z)$ (rather than the density *gradient* profile):

$$\mathrm{SI} = -h_1 \sigma(-h_1) + h_2 \sigma(-h_2) - \int_{-h_2}^{-h_1} \sigma(z) \, \mathrm{d}z. \tag{3}$$

The SI is the amount of buoyancy that must be removed in order for the water column to mix down from depth $-h_1$ to depth $-h_2$ with subsequent uniform density. A stratified layer has a positive SI, a perfectly mixed layer has an SI of zero, and an unstable layer about to overturn has a negative SI. The SI has been used as a measure for stratification in various Mediterranean studies, where it is usually defined with a factor g/ρ_0 so that it is the integral of the Brunt-Väisälä frequency (e.g., Herrmann et al., 2010; L'Hévéder et al., 2013; Somot et al., 2018; Margirier et al., 2020). The partial integration Equation 3 multiplied by -1 has also been used in North Atlantic Studies; Bailey et al. (2005) referred to it as the integrated buoyancy anomaly, and Frajka-Williams et al. (2014) called it the Convection Resistance.

To study the influence of temperature and salinity on the stratification, two additional values of the SI were computed: $\mathrm{SI_T}$ and $\mathrm{SI_S}$, which only consider the contribution of temperature and salinity to stratification, respectively. This was done by using the linear approximation for the density of seawater (Dijkstra, 2008):

$$\rho = \rho_0 \left[1 - \alpha (\Theta - \Theta_0) + \beta (S_A - S_{A,0})\right], \tag{4}$$

where Θ_0 and $S_{A,0}$ are a reference temperature and salinity and $\rho_0 = \rho(\Theta_0, S_{A,0})$ is a reference in-situ density. Furthermore, $\alpha = -\partial\rho/\partial\Theta$ is the thermal expansion coefficient with units 1/K, and $\beta = \partial\rho/\partial S_A$ is the saline contraction coefficient in kg/g. Based on Equation 4, we can view $-\alpha\Theta$ as a first approximation of the temperature contribution to density, and similarly βS_A as the salinity contribution. Hence, replacing σ in Equation 3 by $-\alpha\Theta$ and βS_A, respectively, yields an approximation of the temperature and salinity contribution to stratification, which we denote as $\mathrm{SI_T}$ and $\mathrm{SI_S}$. Note that $-\alpha\Theta$ and βS_A are unitless, so that the stratification contributions $\mathrm{SI_T}$ and $\mathrm{SI_S}$ are given in m instead of kg/m^2. From the time series of salinity, temperature and density profiles averaged over the DCA, monthly values of the SI, $\mathrm{SI_T}$ and $\mathrm{SI_S}$ were computed.

Using the SI, a quantitative measure for restratification could be created as well. The restratification in a certain year was defined to be the increase in SI from the minimum in winter to the maximum in summer. Thus the monthly time series of the SI could be used to compute annual time series of restratification.

3. Results

3.1. The Deep Convection Area

Figure 2 shows maps of the time-mean hydrographic properties in the Irminger Sea. All of these properties are depth-averaged over the upper 600 m, where the variability in density related to convection and restratification is strongest (Figure 3). Below this depth the temporal variations in density become very small; at 600 m the standard deviation in density is only 7.3% of that at the surface. From Figure 2 we can identify the main currents and their characteristics. On the eastern side of the Irminger Sea we find the northward-flowing IC transporting warm and saline water originating from the North Atlantic Current (de Jong et al., 2020; Fried & Jong, 2022). The IC follows the bathymetry, so around 65°N, it veers west and continues southward along the East Greenland Shelf. Alongside this part of the IC we find two currents of Arctic origin, which are thus fresher and colder: the East Greenland Current (EGC) along the shelfbreak and the East Greenland Coastal Current (EGCC) on the inner shelf (e.g., Duyck & De Jong, 2021; Le Bras et al., 2018). The EKE in the Irminger Sea is highest in the IC, in the

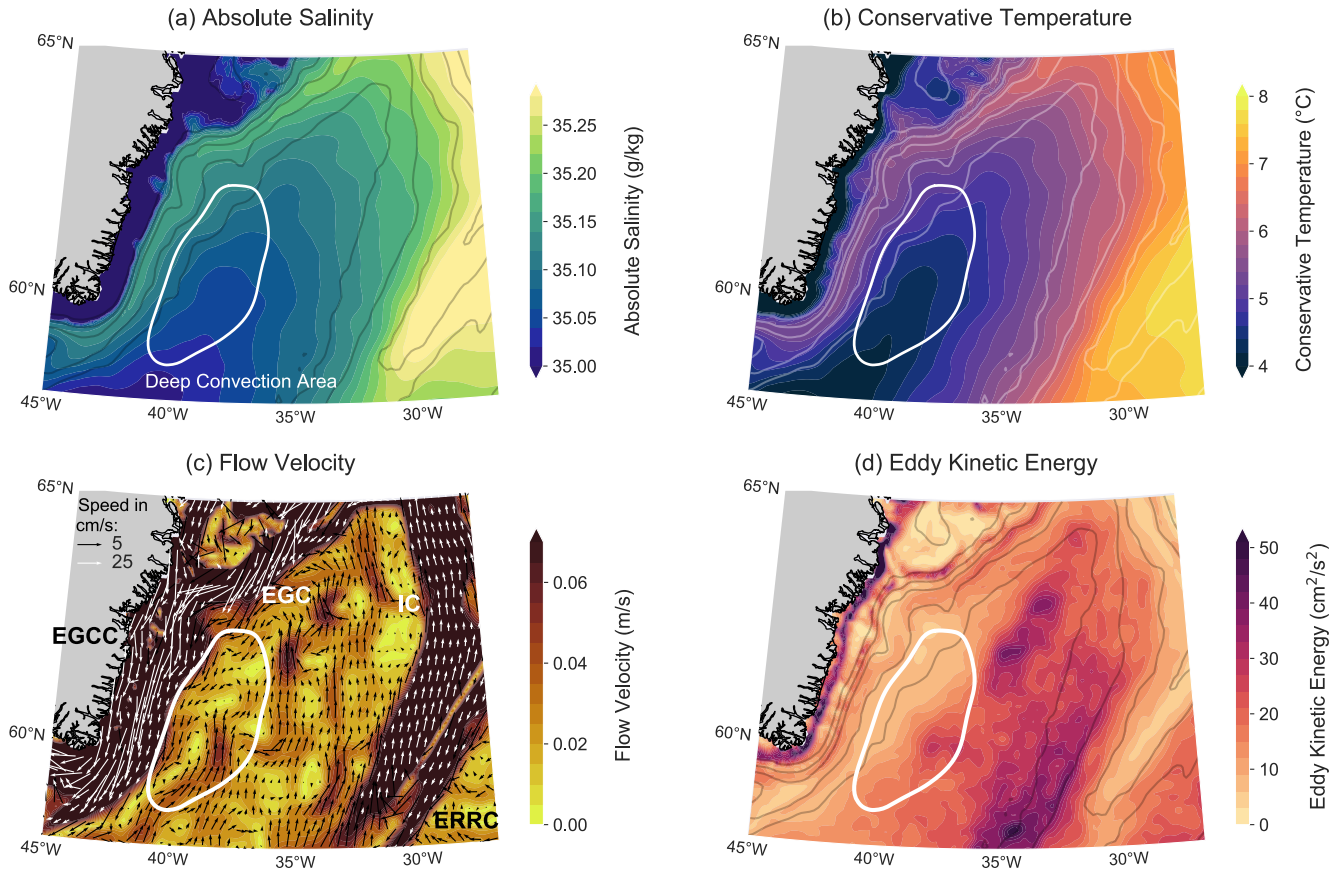

Figure 2. The 1993–2019 mean from the CMEMS reanalysis of the (a) absolute salinity, (b) conservative temperature, (c) flow velocity and (d) eddy kinetic energy in the Irminger Sea, averaged over the upper 600 m of the ocean. The white contour indicates the boundary of the Deep Convection Area. In panels (a), (b), and (d), smoothed contours of the bathymetry between 500 and 2500 m are shown at 500 m intervals. In panel (c), velocity direction and magnitude are indicated by vectors. Velocities smaller than 0.07 m/s are indicated by black arrows, larger velocities by white arrows. The black and white vectors have different scalings, as shown by the reference vectors in the top right of the panel. In this panel the different currents are indicated: EGCC = East Greenland Coastal Current; EGC = East Greenland Current; IC = Irminger Current; ERRC = East Reykjanes Ridge Current.

EGCC and to the northeast of the DCA. These regions are in agreement with the strong EKE regions that were derived from surface drifter data by Fratantoni (2001) and from satellite altimetry data by Volkov (2005) and Fan et al. (2013). Eddies observed in the central Irminger Sea are anticyclonic and have a warm and saline core, which suggests that they are shed by the IC. Fan et al. (2013) found that the mean core diameter of 16 eddies observed between 2002 and 2009 was 12 km. The CMEMS reanalysis has a spatial resolution of 1/12°, which is about 9 km in the latitudinal direction and 4.5 km in the longitudinal direction in the DCA. Thus the resolution is likely high enough to resolve the larger Irminger Sea anticyclones, but the smaller ones might be missed, meaning the EKE might be underrepresented in the reanalysis.

To study the interannual variability and vertical structure of hydrographic properties in the DCA, we consider the full 1993–2019 time series of spatially averaged profiles of DCA salinity, temperature and density (Figure 3). The mean and maximum MLD over the DCA are also shown. The temperature and density have monotonously stratified structures, with warm, buoyant layers above cold, dense ones. By contrast, salinity has a mid-depth minimum in the layer between 500 and 1,500 m, which is the signature of convectively formed water. From the evolution of the MLD we see that there is strong interannual variability in the convection strength. There is also interannual variability in stratification: some years have much weaker vertical density gradients than other years. In the early 1990s, cold and stormy winters forced the deepest mixed layers of the time series (Våge et al., 2011), which led to weak vertical density gradients and outcropping of isopycnals. In the 2000s, mixed layers were shallower, and the DCA was more stratified. From 2015 until 2018, the MLD increased again, resulting in a thickening of deep cold and dense layers and thus a decrease in stratification. The largest temporal fluctuations in hydrographic properties are found in the upper 600 m of the water column (right column of Figure 3), on which we will focus.

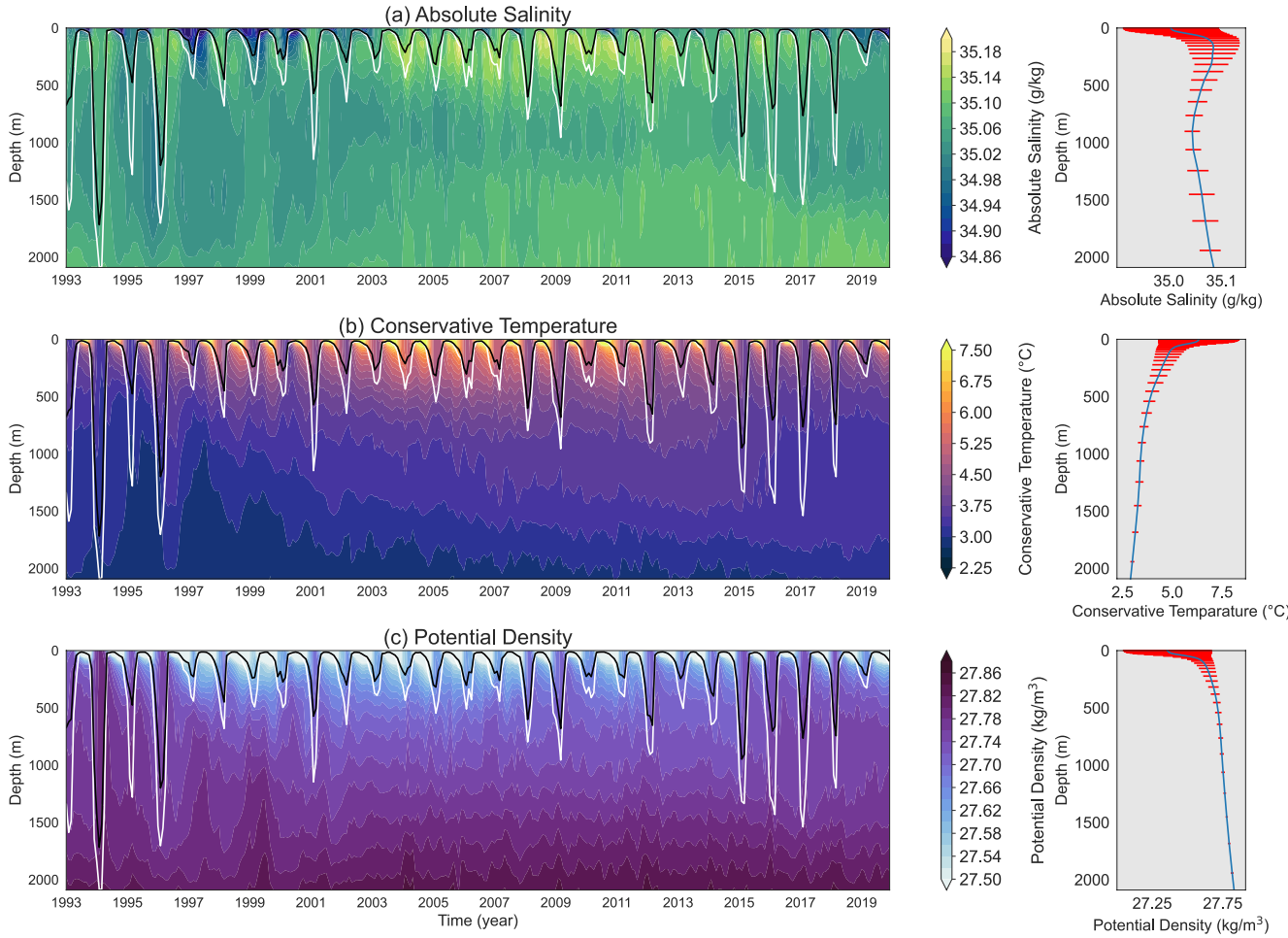

Figure 3. The temporal evolution of profiles of (a) absolute salinity, (b) conservative temperature and (c) potential density from the CMEMS reanalysis averaged over the Deep Convection Area (DCA). The mixed layer depth averaged over the DCA is shown in black; the maximum mixed layer depth reached within the DCA is shown in white. The panels on the right show the 1993–2019 time-mean (blue curve) and standard deviations (red bars) of each variable.

3.2. Structure and Variability of Restratification

To see how properties within the DCA generally vary throughout the year, we composed climatologies of the salinity, temperature and density profiles in the upper 600 m of the DCA (Figure 4). A seasonal cycle consisting of deepening convection in autumn and winter, followed by restratification in spring and summer, is clearly visible in all three variables. The deepest mixed layers are typically reached in February through April (although a few years with shallower convection imprint as a slight non-zero vertical gradient in the climatology). Restratification sets in April and May, with the halocline, thermocline and pycnocline steepening through to August (for temperature and density) and September (for salinity). The uppermost 30–50 m of the water column is typically characterized by a wind-mixed layer (Sampe & Xie, 2007). The salinity climatology (Figure 4a) shows different behavior in the upper and lower parts of the water column. In summer, the surface layer freshens, likely through precipitation and freshwater from the Greenland shelf (Duyck & De Jong, 2021; Duyck et al., 2022). The deeper part of the water column is dominated by lateral exchange with the perimeter of the Irminger Sea, where salinity is generally higher than in the DCA (Figure 2a). In winter, convection homogenizes the salinity over the upper and lower layer, making the former saltier and the latter fresher. The temperature and density climatologies (Figures 4b and 4c) exhibit the same sign in change over the upper 600 m, but a difference in timing and magnitude in restratification in the upper and lower layer can still be observed. In the upper layer, the increase in temperature is much stronger and maximum temperatures are reached in August. This stronger warming is likely the effect of heat gain through atmospheric surface fluxes (Figure 5). In the lower layer, the temperature gradient remains substantially weaker and warming continues until November, as is expected from warming by

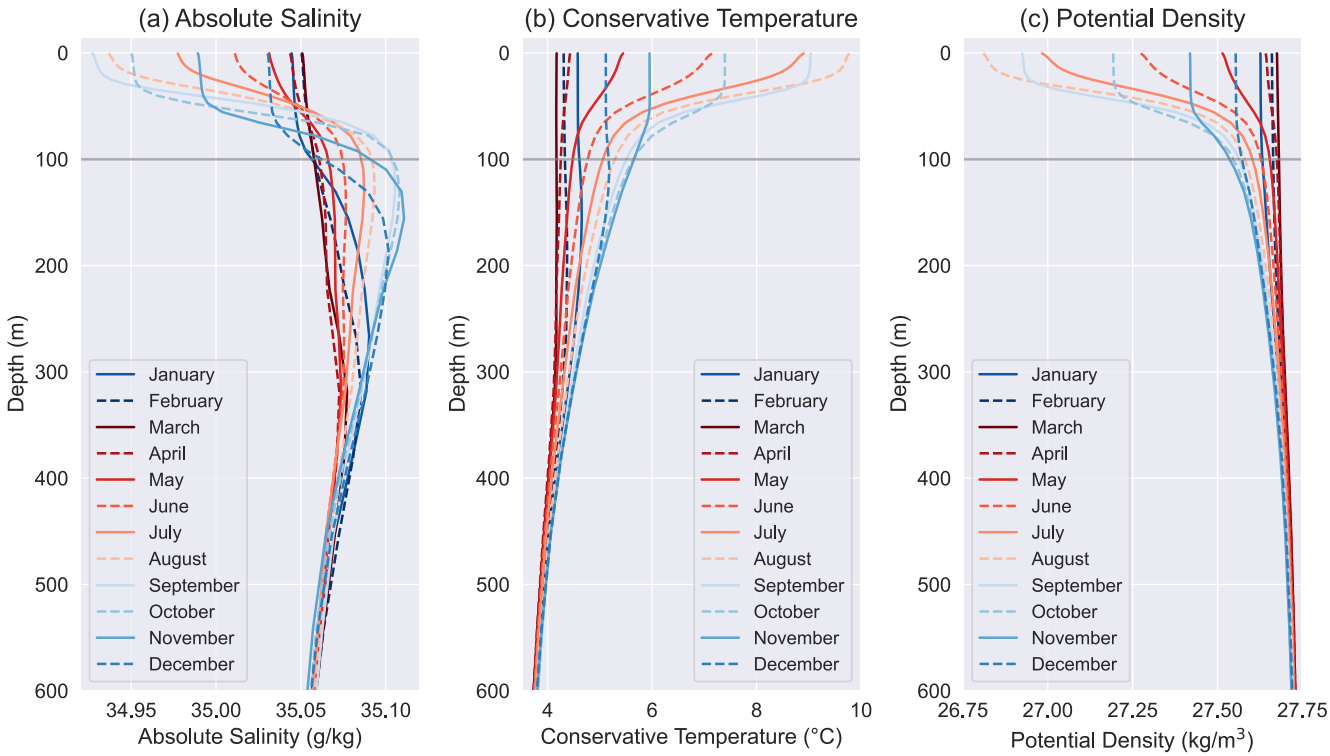

Figure 4. Climatologies of the (a) absolute salinity, (b) conservative temperature and (c) potential density profiles averaged over the Deep Convection Area, from the monthly 1993–2019 CMEMS reanalysis.

lateral exchange with warmer waters (Figure 2b). The net effect of temperature and salinity is a strong increase in the stable density gradient in the upper layer during summer and a weaker, delayed increase below (Figure 4c). Given the different behavior in restratification in the upper layer down to 100 m and the lower layer below (down to 600 m), we will study the interannual variability in these layers separately.

The stratification index of the two layers is shown in Figure 5, together with the climatology of the MLD, the net surface heat flux and the net surface freshwater flux. The SI climatology shows the difference in timing described

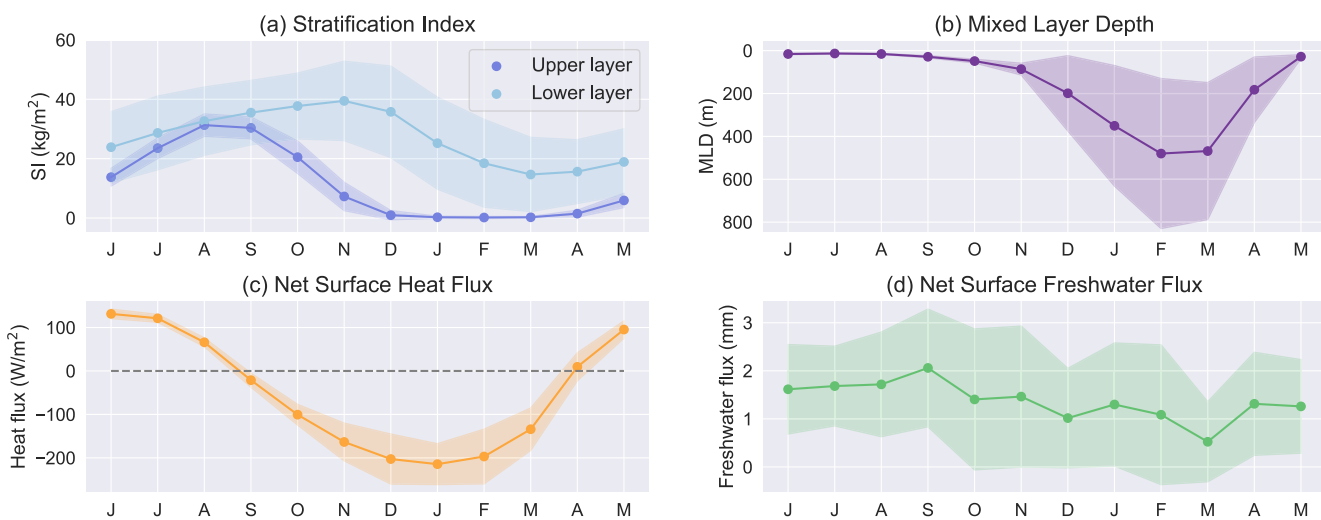

Figure 5. Climatologies of the (a) stratification index in the upper (0–100 m) and lower (100–600 m) layer, (b) mixed layer depth, (c) net surface heat flux and (d) net surface freshwater flux averaged over the Deep Convection Area. The data of (a) and (b) are from the monthly 1993–2019 CMEMS reanalysis, the data of (c) and (d) are from the monthly 1993–2019 ERA5 reanalysis. The shaded areas indicate the standard deviations.

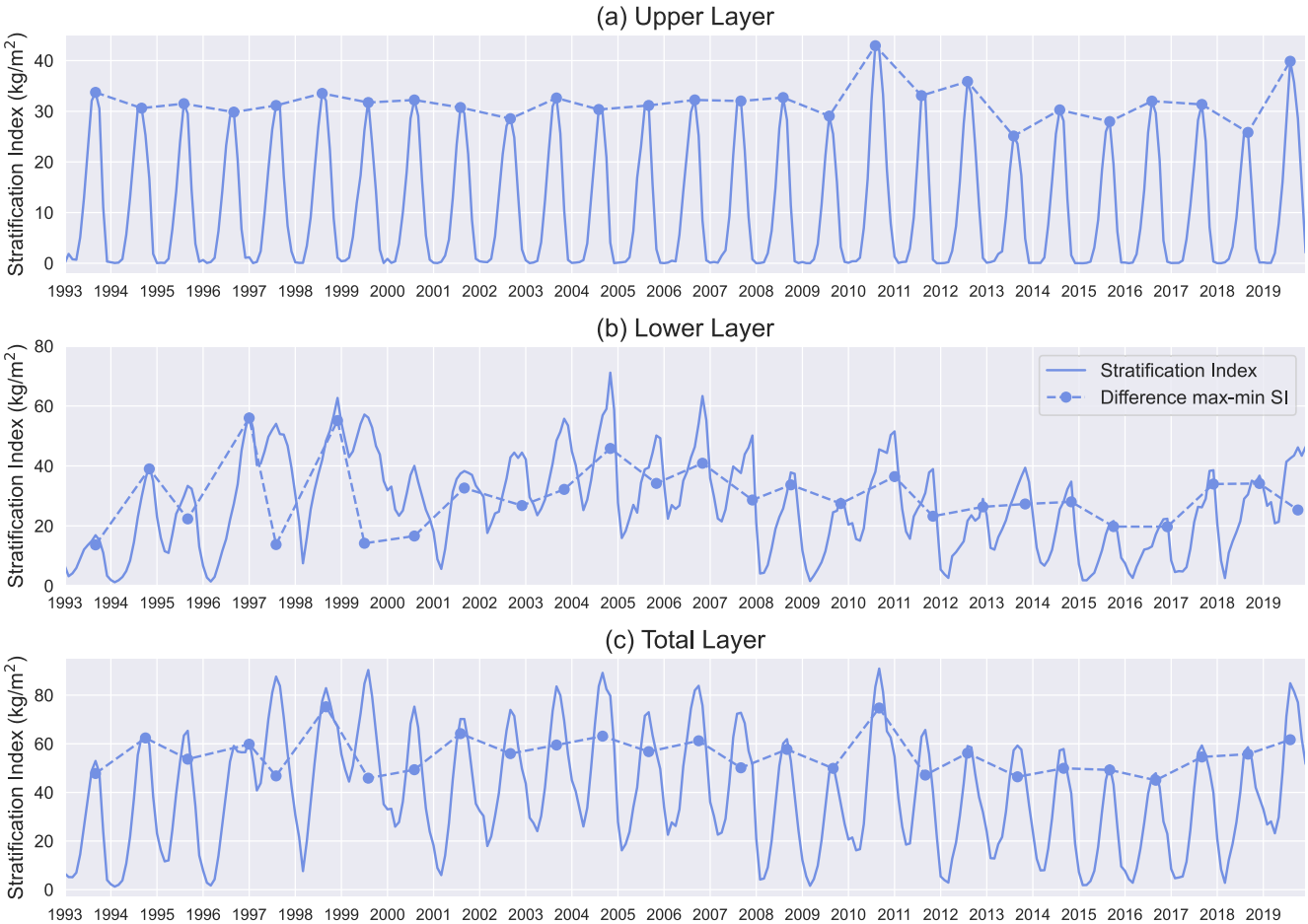

Figure 6. The stratification index (SI) time series in the Deep Convection Area for (a) the upper layer from 0 to 100 m, (b) the lower from 100 to 600 m, and (c) the total (upper + lower) layer from 0 to 600 m. The dashed line shows the annual values of the restratification, defined as the increase in SI from the minimum in winter to the maximum in summer. Note the different vertical scales of the panels.

above. Additionally, the lower layer SI has a larger standard deviation, indicating stronger interannual variability. Increasing upper layer SI matches with periods of surface heating and decreasing upper layer SI with surface cooling. Timing in lower layer SI matches with the MLD as expected. The net surface freshwater flux is highly variable, but generally is higher in summer than in winter, which can add to the summer freshening of the upper layer. This is discussed further in relation to the interannual variability in Section 3.3.

The time series of SI and restratification from 1993 to 2019 (Figure 6) show the difference in interannual variability in the upper, lower and total (upper + lower) layer. The upper layer stratification is dominated by the seasonal cycle, with very little interannual variability in either SI or restratification. Two years (2010 and 2019) stand out as having higher summer maxima and thus high restratification, and we will come back to these in Section 3.3.2. In the lower layer there is still a strong seasonal cycle, but also notable interannual variability. Unlike in the upper layer, where the SI is set to zero each winter, the lower layer has a memory of stratification and mixing over previous years. The restratification in the lower layer also shows interannual variability. The values of both the SI and the restratification are in general higher in the lower layer than in the upper layer because more buoyancy is stored in this thicker layer (Equation 2). The stratification over the total layer (from 0 to 600 m) is the superposition of the strong seasonal cycle in both layers and the interannual variability in the lower layer. The values of the SI and restratification are comparable in magnitude to those in the lower layer.

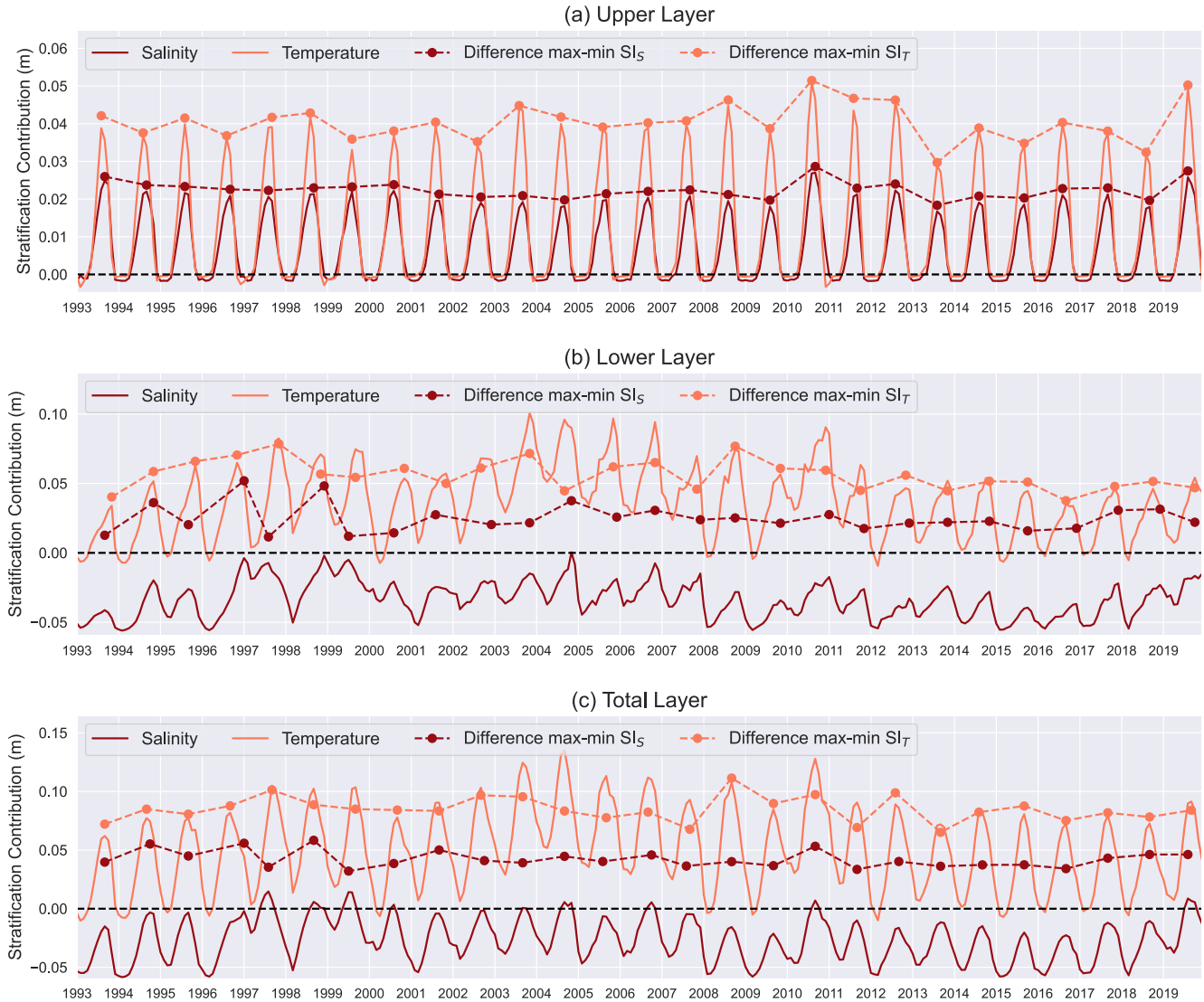

Figure 7. The stratification contribution of salinity and temperature in the Deep Convection Area for (a) the upper layer from 0 to 100 m, (b) the lower from 100 to 600 m, and (c) the total water layer from 0 to 600 m. The dashed lines show the annual values of the restratification, defined as the increase in stratification contribution from the minimum in winter to the maximum in summer. Note the different vertical scales of the panels.

3.3. Physical Processes Contributing to Restratification

3.3.1. Role of Salinity and Temperature in Restratification

The climatology in Figure 4 suggested there are different roles for temperature and salinity in restratification. To study these further, we investigate time series of the SI_T and SI_S as introduced in Section 2.2.2 (Figure 7). In the upper layer, the SI_T and SI_S both follow a strong seasonal cycle. Values are slightly negative in winter indicating unstable stratification during convection and positive for the remainder of the year due to higher temperatures and lower salinities. In the lower layer the SI_S is always negative, indicating the destabilizing effect of salinity (saline water over fresher water) seen also in Figure 4a. Despite the stable, fresh upper layer, the effect of salinity over the total 0–600 m layer is destabilizing. Since the temperature exhibits the same sign gradient over both layers, the effect of temperature is always stabilizing except during some winter months with deep mixed layers (cf. Figure 3). In the lower layer, temperature and salinity co-vary as the restratifying waters from the perimeter are warm and saline (Pearson correlation coefficient between the deseasonalized time series of SI_S and SI_T is 0.60, with $p \ll 0.01$). This is not necessarily so for the upper layer, where heat and freshwater fluxes can vary independently. Even so, the correlation between the variability in SI_S and SI_T is quite strong (Pearson correlation

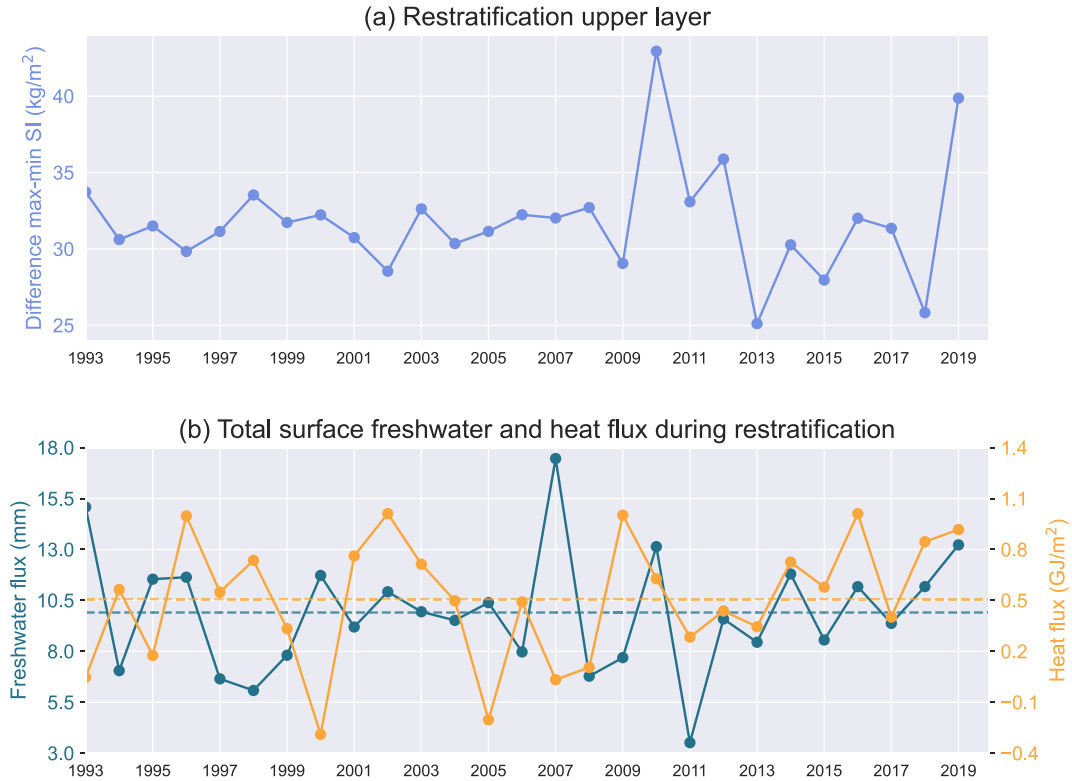

Figure 8. Annual time series of (a) restratification and (b) total accumulated surface freshwater and heat flux during the restratification period in the upper layer over the Deep Convection Area. The restratification period starts in the month after the occurrence of the minimum winter stratification index (SI) and ends in the month of the next maximum SI in the upper layer. The dashed horizontal lines show the time-mean values of the depicted time series.

coefficient between deseasonalized time series is 0.64, $p \ll 0.01$). From the yearly restratification contributions in Figure 7 it can be seen that the restratification contribution of temperature (light dashed line) is always larger than that of salinity (dark dashed line) in absolute value.

3.3.2. Role of Surface Fluxes and Lateral Fluxes in Restratification

The climatology from Figure 5 suggested a relation between upper layer stratification and atmospheric surface fluxes. Therefore we investigate interannual variability in surface heat and freshwater fluxes over the period of restratification, from the winter minimum SI in the upper layer to the next summer maximum of each year. Figure 8 shows the spring/summer accumulated atmospheric freshwater and heat fluxes together with the annual upper layer restratification. The total atmospheric buoyancy flux is almost entirely determined by the atmospheric heat flux. The restratification is not significantly correlated with either the surface freshwater flux nor with the heat flux separately (Pearson r of restratification and annual freshwater flux is 0.24, p-value 0.23; Pearson r of restratification and annual heat flux is −0.064, p-value 0.75). However, in years when both are stronger than average, they may reinforce each other. The presence of a fresh surface layer, which already increases stratification, restricts warming by the high heat flux to a thin layer, resulting in higher temperatures and very high stratification by the end of summer (Oltmanns et al., 2018). A reinforcement of strong heat and freshwater fluxes appears to be the case for the years with the highest restratification values, 2010 and 2019. Both years were characterized by above-average freshwater and heat gain during the restratification period, with the high freshwater gain mainly due to low evaporation (not shown here). The reverse does not appear to be true; years with below-average heat and freshwater fluxes do not exhibit much weaker restratification. Moreover, higher freshwater and heat flux does not always coincide with more restratification; compare, for example, the years 2017 and 2018 in Figure 8. Thus, there is no linear relationship between surface fluxes and restratification in the upper layer. Although very strong fluxes of both freshwater and heat may reinforce each other and result in strong restratification, there are likely other processes playing a major role in restratifying the upper layer.

In the lower layer, as opposed to the upper layer, there is strong interannual variability in both the summer SI and the winter SI (Figure 6b). The winter stratification is directly affected by the depth of the mixed layer; there is a significant correlation between the annual winter minimum SI and maximum MLD, with a Pearson r of −0.68 and $p \ll 0.01$. However, even though the MLD influences the winter minimum SI and therewith the restratification, there is no significant correlation between the maximum MLD and the restratification in the lower layer (Pearson r of 0.27, p-value 0.18; Figure 9a).

During spring and summer the lower layer is isolated from the upper layer, so the lower layer restratification is less affected by surface fluxes and more by lateral advection of buoyant water from the perimeter of the Irminger Sea. Since this advection must cross the streamlines of the Irminger Gyre to enter the DCA, it is likely facilitated by eddies. Lateral advection by eddies appears to be supported by the significant correlation between the time series of lower layer restratification and mean surface EKE in the eastern Irminger Sea during restratification (Figure 9b; Pearson r of 0.66, $p \ll 0.01$). The EKE time series is averaged along the WOCE AR7E line (Koltermann et al., 2011) starting at the eastern DCA boundary at 315 km (Figures 9c and 9d), where the highest EKE values are found. The eddies from the eastern Irminger Sea bring warm and saline IC water into the DCA (Fan et al., 2013); this further supports the notion that IC eddies drive lower layer restratification. Enhanced EKE values are also found west of the DCA (Figures 9c and 9d); however, no significant correlation was found between the lower layer restratification and the surface EKE west of the DCA during restratification (Pearson r of 0.052, $p = 0.8$).

4. Discussion and Conclusions

To summarize our results, most of the variability in stratification in the central Irminger Sea is located in the upper 600 m of the water column. We found distinctly different variability in stratification in the upper 100 m and the 100–600 m layer. In the upper layer, there is a strong seasonal cycle with freshening and warming in spring and summer and very little interannual variability. Exceptionally high upper layer stratification may be reached in years when both heat and freshwater fluxes are above average. However, the surface fluxes alone cannot explain the restratification in the upper layer. In the lower layer, there is substantial interannual variability in stratification. The winter minimum stratification is determined by the strength of convection: deeper mixed layers lead to weaker stratification. The restratification after winter is strongly linked to the EKE in the eastern Irminger Sea, suggesting that warm, saline eddies shed by the IC play an important role in restratifying the DCA.

This two layer structure in restratification in the Irminger Sea is very similar to what is observed in the Labrador Sea (Straneo, 2006a), which also displays surface freshening during restratification while the layer below gets more saline. However, there is an important difference. At least part of the two layer structure of restratification in the Labrador Sea is derived from the two layer eddies shed from the boundary current. These eddies have a cold and fresh upper layer extending until 100–400 m depth and a warm and saline layer below (de Jong et al., 2014; Hátún et al., 2007; Lilly et al., 1999). However, in the Irminger Sea no eddies with a fresh top are observed. The eddies originating from the IC are warm and saline throughout (Fan et al., 2013). The high EKE region west of the DCA (Figure 2d) does not seem to generate eddies with a fresh cap that influence the Irminger Sea restratification. Either the EKE in this region is related to a circulation response to the wind that does not consist of coherent eddies (Duyck et al., 2022), or eddies formed in this region tend to move westward and will be quickly advected by the EGC, thus being unable to enter the convective region. As opposed to the Labrador Sea, in the Irminger Sea the upper layer freshening is due to surface freshwater gain and thin layers of freshwater driven off the East Greenland shelf during strong wind events (Duyck et al., 2022).

Amplification of upper layer stratification through co-occurring above normal surface heat and freshwater gain was seen in 2010 and 2019. The 2010 event was described by Oltmanns et al. (2018). They speculate that the fresh surface layer might have had an additional continental origin. They found that surface temperatures were high in a broad area near the southeast Greenland shelf, where glacier melt would be accelerated. Freshening due to ice melt is a plausible cause for freshwater anomalies near the East Greenland shelf, which we know can be exported to the DCA (Duyck & De Jong, 2021; Duyck et al., 2022; Foukal et al., 2020) and thus increase the stratification there. In 2019 runoff from Greenland was high was well (Slater et al., 2021), but there was also an additional cause for the high stratification: a strong freshwater anomaly that formed between 2012 and 2016 in the eastern subpolar North Atlantic, as described by Holliday et al. (2020). This anomaly went on to propagate northwards into the Irminger Sea, the Labrador Sea and the Nordic Seas. Its effects can be seen in the freshening

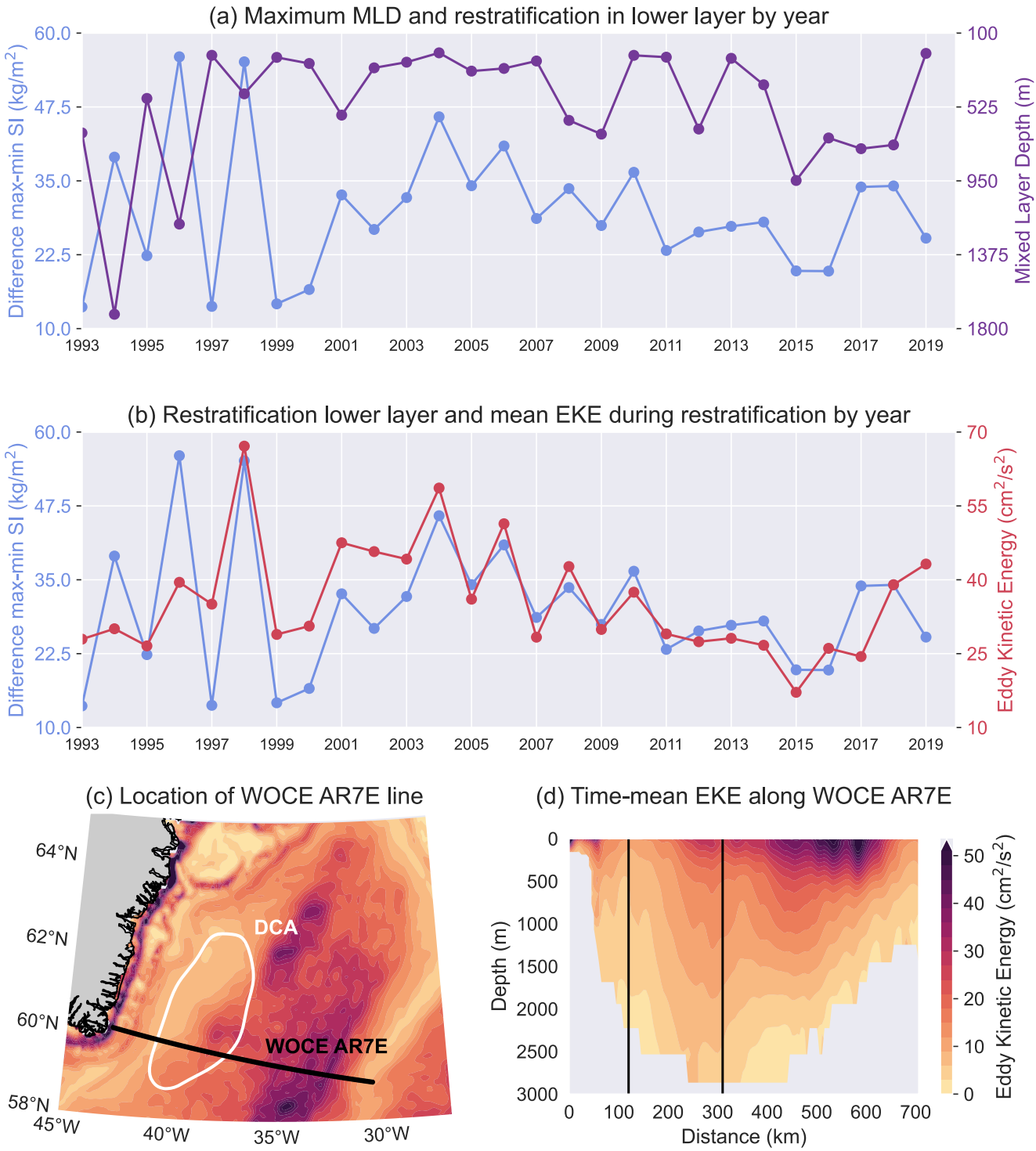

Figure 9. (a) Maximum mixed layer depth and restratification in the lower layer of the Deep Convection Area (DCA). (b) Restratification in the lower layer of the DCA and surface eddy kinetic energy (EKE) along the WOCE AR7E section eastward of the DCA, averaged over the restratification phase. The restratification period starts in the month after the occurrence of the minimum winter stratification and ends in the month of the next maximum stratification in the upper layer. (c) The WOCE AR7E line in the Irminger Sea (Koltermann et al., 2011) and the boundary of the DCA, plotted on top of the 1993–2019 mean EKE field averaged over the upper 600 m. (d) The 1993–2019 mean from the CMEMS reanalysis of the EKE along the WOCE AR7E line. The vertical black lines mark the points where the line intersects the DCA boundary.

of the upper and intermediate layers in the Irminger Sea from 2017 onwards (Figure 3a) as well as in the high stratification in 2019 (Figure 6a). In the long term, anthropogenic climate change is expected to further enhance Greenland ice melt. Upper layer stratification increases as seen in 2010 and 2019 may occur more frequently and stronger. Further studies are needed to understand the extent to which Greenland ice melt and meltwater export might influence stratification in the Irminger Sea in the future.

The lower layer displays much stronger interannual variability, partly through longer ocean memory (set by convection in previous winters) and partly through differences in restratification. We found a strong relation between the strength of the annual restratification and the EKE in the eastern Irminger Sea. Anticyclonic eddies with warm and saline cores shed by the IC move westward into the DCA, thus restratifying it. In the Labrador Sea, eddies play a crucial role both in determining the location of the deep convection region (Chanut et al., 2008) as well as in the downwelling and export of convective waters (Georgiou et al., 2019). As the Irminger Sea is an important contributor to the overturning in the subpolar gyre (Li et al., 2021; Lozier et al., 2019; Petit et al., 2020) it is imperative that eddy processes and their contribution to restratification in the Irminger Sea are better understood.

Data Availability Statement

The CMEMS monthly mean data is available at https://resources.marine.copernicus.eu/product-detail/GLOBAL_MULTIYEAR_PHY_001_030/DATA-ACCESS. The files for 1993–2012 were last accessed on 29 October 2020; the files for 2013–2019 were last accessed on 21 May 2021. The ERA5 monthly averaged data on single levels is available at https://cds.climate.copernicus.eu/cdsapp#!/dataset/reanalysis-era5-single-levels-monthly-means?tab=overview and was last accessed on 16 September 2021. Data was processed using Python 3.6.13. All code used for processing data and making figures for this study is available at https://github.com/MiriamSterl/RestratificationIrmingerSea.

Acknowledgments
This work was financially supported by the Innovational Research Incentives Scheme of the Netherlands Organisation for Scientific Research (NWO) under grant agreement no. 016.Vidi.189.130.

References

Bailey, D. A., Rhines, P. B., & Häkkinen, S. (2005). Formation and pathways of North Atlantic deep water in a coupled ice–ocean model of the Arctic–North Atlantic Oceans. *Climate Dynamics*, *25*(5), 497–516. https://doi.org/10.1007/s00382-005-0050-3

Brown, P. J., McDonagh, E. L., Sanders, R., Watson, A. J., Wanninkhof, R., King, B. A., et al. (2021). Circulation-driven variability of Atlantic anthropogenic carbon transports and uptake. *Nature Geoscience*, *14*(8), 571–577. https://doi.org/10.1038/s41561-021-00774-5

Chanut, J., Barńier, B., Large, W., Debreu, L., Penduff, T., Molines, J. M., & Mathiot, P. (2008). Mesoscale eddies in the Labrador Sea and their contribution to convection and restratification. *Journal of Physical Oceanography*, *38*(8), 1617–1643. https://doi.org/10.1175/2008JPO3485.1

Cuny, J., Rhines, P. B., Niiler, P. P., & Bacon, S. (2002). Labrador Sea boundary currents and the fate of the Irminger Sea Water. *Journal of Physical Oceanography*, *32*(2), 627–647. https://doi.org/10.1175/1520-0485(2002)032⟨0627:LSBCAT⟩2.0.CO;2

de Jong, M. F., Aken, H. M. V., Våge, K., & Pickart, R. S. (2012). Convective mixing in the central Irminger Sea: 2002-2010. *Deep-Sea Research Part I Oceanographic Research Papers*, *63*, 36–51. https://doi.org/10.1016/j.dsr.2012.01.003

de Jong, M. F., Bower, A. S., & Furey, H. H. (2014). Two years of observations of warm-core anticyclones in the Labrador Sea and their seasonal cycle in heat and salt stratification. *Journal of Physical Oceanography*, *44*(2), 427–444. https://doi.org/10.1175/JPO-D-13-070.1

de Jong, M. F., Bower, A. S., & Furey, H. H. (2016). Seasonal and interannual variations of Irminger ring formation and boundary-interior heat exchange in FLAME. *Journal of Physical Oceanography*, *46*(6), 1717–1734. https://doi.org/10.1175/JPO-D-15-0124.1

de Jong, M. F., & de Steur, L. (2016). Strong winter cooling over the Irminger Sea in winter 2014–2015, exceptional deep convection, and the emergence of anomalously low SST. *Geophysical Research Letters*, *43*(13), 7106–7113. https://doi.org/10.1002/2016GL069596

de Jong, M. F., de Steur, L., Fried, N., Bol, R., & Kritsotalakis, S. (2020). Year-round measurements of the Irminger Current: Variability of a two-core current system observed in 2014–2016. *Journal of Geophysical Research: Oceans*, *125*(10). https://doi.org/10.1029/2020JC016193

de Jong, M. F., Oltmanns, M., Karstensen, J., & de Steur, L. (2018). Deep convection in the Irminger Sea observed with a dense mooring array. *Oceanography*, *31*(1), 50–59. https://doi.org/10.5670/oceanog.2018.109

Dijkstra, H. A. (2008). *Dynamical oceanography*. Springer US. https://doi.org/10.1007/978-3-540-76376-5

Drévillon, M., Fernandez, E., & Lellouche, J. M. (2021). Product user manual for the global ocean physical multi year product GLOBAL_MULTIYEAR_PHY_001_030. Retrieved from https://catalogue.marine.copernicus.eu/documents/PUM/CMEMS-GLO-PUM-001-030.pdf

Duyck, E., & De Jong, M. F. (2021). Circulation over the south-east Greenland shelf and potential for liquid freshwater export: A drifter study. *Geophysical Research Letters*, *48*(5), 1–9. https://doi.org/10.1029/2020GL091948

Duyck, E., Gelderloos, R., & Jong, M. F. (2022). Wind-driven freshwater export at Cape Farewell. *Journal of Geophysical Research: Oceans*, *127*(5). https://doi.org/10.1029/2021jc018309

England, M. H. (1995). The age of water and ventilation timescales in a global ocean model. *Journal of Physical Oceanography*, *25*(11), 2756–2777. https://doi.org/10.1175/1520-0485(1995)025<2756:taowav>2.0.co;2

Fan, X., Send, U., Testor, P., Karstensen, J., & Lherminier, P. (2013). Observations of Irminger Sea anticyclonic eddies. *Journal of Physical Oceanography*, *43*(4), 805–823. https://doi.org/10.1175/JPO-D-11-0155.1

Foukal, N. P., Gelderloos, R., & Pickart, R. S. (2020). A continuous pathway for fresh water along the East Greenland shelf. *Science Advances*, *6*(43). https://doi.org/10.1126/sciadv.abc4254

Fox-Kemper, B., Hewitt, H. T., Xiao, C., Adalgeirsdóttir, G., Drijfhout, S. S., Edwards, T. L., et al. (2021). *Ocean, cryosphere and sea level change*. Cambridge University Press. https://doi.org/10.1017/9781009157896.011

Frajka-Williams, E., Rhines, P. B., & Eriksen, C. C. (2014). Horizontal stratification during deep convection in the Labrador Sea. *Journal of Physical Oceanography*, *44*(1), 220–228. https://doi.org/10.1175/JPO-D-13-069.1

Fratantoni, D. M. (2001). North Atlantic surface circulation during the 1990's observed with satellite-tracked drifters. *Journal of Geophysical Research*, *106*(C10), 22067–22093. https://doi.org/10.1029/2000jc000730

Fried, N., & Jong, M. F. (2022). The role of the Irminger Current in the Irminger Sea northward transport variability. *Journal of Geophysical Research: Oceans*, *127*(3). https://doi.org/10.1029/2021JC018188

Fröb, F., Olsen, A., Våge, K., Moore, G. W., Yashayaev, I., Jeansson, E., & Rajasakaren, B. (2016). Irminger Sea deep convection injects oxygen and anthropogenic carbon to the ocean interior. *Nature Communications*, *7*(13244), 13244. https://doi.org/10.1038/ncomms13244

Gelderloos, R., Katsman, C. A., & Drijfhout, S. S. (2011). Assessing the roles of three eddy types in restratifying the Labrador Sea after deep convection. *Journal of Physical Oceanography*, *41*(11), 2102–2119. https://doi.org/10.1175/JPO-D-11-054.1

Georgiou, S., van der Boog, C. G., Brüggemann, N., Ypma, S. L., Pietrzak, J. D., & Katsman, C. A. (2019). On the interplay between downwelling, deep convection and mesoscale eddies in the Labrador Sea. *Ocean Modelling*, *135*, 56–70. https://doi.org/10.1016/j.ocemod.2019.02.004

Hátún, H., Eriksen, C. C., & Rhines, P. B. (2007). Buoyant eddies entering the Labrador Sea observed with gliders and altimetry. *Journal of Physical Oceanography*, *37*(12), 2838–2854. https://doi.org/10.1175/2007JPO3567.1

Herrmann, M., Sevault, F., Beuvier, J., & Somot, S. (2010). What induced the exceptional 2005 convection event in the northwestern Mediterranean basin? Answers from a modeling study. *Journal of Geophysical Research*, *115*(C12), 1–19. https://doi.org/10.1029/2010JC006162

Hersbach, H., Bell, B., Berrisford, P., Hirahara, S., Horányi, A., Muñoz-Sabater, J., et al. (2020). The ERA5 global reanalysis. *Quarterly Journal of the Royal Meteorological Society*, *146*(730), 1999–2049. https://doi.org/10.1002/qj.3803

Holliday, N. P., Bersch, M., Berx, B., Chafik, L., Cunningham, S., Florindo-López, C., et al. (2020). Ocean circulation causes the largest freshening event for 120 years in eastern subpolar North Atlantic. *Nature Communications*, *11*(1), 585. https://doi.org/10.1038/s41467-020-14474-y

Jones, H., & Marshall, J. (1997). Restratification after deep convection. *Journal of Physical Oceanography*, *27*(10), 2276–2287. https://doi.org/10.1175/1520-0485(1997)027⟨2276:RADC⟩2.0.CO;2

Katsman, C. A., Drijfhout, S. S., Dijkstra, H. A., & Spall, M. A. (2018). Sinking of dense North Atlantic waters in a global ocean model: Location and controls. *Journal of Geophysical Research: Oceans*, *123*(5), 3563–3576. https://doi.org/10.1029/2017JC013329

Katsman, C. A., Spall, M. A., & Pickart, R. S. (2004). Boundary current eddies and their role in the restratification of the Labrador Sea. *Journal of Physical Oceanography*, *34*(9), 1967–1983. https://doi.org/10.1175/1520-0485(2004)034⟨1967:BCEATR⟩2.0.CO;2

Koltermann, K., Gouretski, V., & Jancke, K. (2011). In J. G. M. Sparrow, & P. Chapman (Ed.), *Hydrographic atlas of the world ocean circulation experiment (WOCE), Volume 3: Atlantic Ocean*.

Lazier, J., Hendry, R., Clarke, A., Yashayaev, I., & Rhines, P. (2002). Convection and restratification in the Labrador Sea, 1990-2000. *Deep-Sea Research Part I Oceanographic Research Papers*, *49*(10), 1819–1835. https://doi.org/10.1016/S0967-0637(02)00064-X

Le Bras, I. A., Straneo, F., Holte, J., de Jong, M. F., & Holliday, N. P. (2020). Rapid export of waters formed by convection near the Irminger Sea's western boundary. *Geophysical Research Letters*, *47*(3). https://doi.org/10.1029/2019GL085989

Le Bras, I. A., Straneo, F., Holte, J., & Holliday, N. P. (2018). Seasonality of freshwater in the east Greenland current system from 2014 to 2016. *Journal of Geophysical Research: Oceans*, *123*(12), 8828–8848. https://doi.org/10.1029/2018JC014511

L'Hévéder, B., Li, L., Sevault, F., & Somot, S. (2013). Interannual variability of deep convection in the Northwestern Mediterranean simulated with a coupled AORCM. *Climate Dynamics*, *41*(3–4), 937–960. https://doi.org/10.1007/s00382-012-1527-5

Li, F., Lozier, M. S., Holliday, N. P., Johns, W. E., Le Bras, I. A., Moat, B. I., et al. (2021). Observation-based estimates of heat and freshwater exchanges from the subtropical North Atlantic to the Arctic. *Progress in Oceanography*, *197*, 102640. https://doi.org/10.1016/j.pocean.2021.102640

Lilly, J. M., Rhines, P. B., Visbeck, M., Davis, R., Lazier, J. R., Schott, F., & Farmer, D. (1999). Observing deep convection in the Labrador Sea during winter 1994/95. *Journal of Physical Oceanography*, *29*(8), 2065–2098. https://doi.org/10.1175/1520-0485(1999)029⟨2065:odcitl⟩2.0.co;2

Lozier, M. S., Li, F., Bacon, S., Bahr, F., Bower, A. S., Cunningham, S. A., et al. (2019). A sea change in our view of overturning in the subpolar North Atlantic. *Science*, *363*(6426), 516–521. https://doi.org/10.1126/science.aau6592

Madec, G. (2016). NEMO ocean engine. https://doi.org/10.5281/zenodo.3248739

Margirier, F., Testor, P., Heslop, E., Mallil, K., Bosse, A., Houpert, L., et al. (2020). Abrupt warming and salinification of intermediate waters interplays with decline of deep convection in the Northwestern Mediterranean Sea. *Scientific Reports*, *10*, 1–11. https://doi.org/10.1038/s41598-020-77859-5

Marshall, J., & Schott, F. (1999). Open-ocean convection: Observations, theory, and models. *Reviews of Geophysics*, *37*, 1–64. https://doi.org/10.1029/98rg02739

McCarthy, G. D., Smeed, D. A., Cunningham, S. A., & Roberts, C. D. (2017). Atlantic meridional overturning circulation. In *Marine climate change impacts partnership: Science review* (pp. 15–21). https://doi.org/10.14465/2017.arc10.002-atl

McDougall, T. J., & Barker, P. (2011). Getting started with TEOS-10 and the Gibbs seawater (GSW) oceanographic toolbox. SCOR/IAPSO WG127. Retrieved from http://www.teos-10.org/pubs/gsw/v3_04/pdf/Getting_Started.pdf

Oltmanns, M., Karstensen, J., & Fischer, J. (2018). Increased risk of a shutdown of ocean convection posed by warm North Atlantic summers. *Nature Climate Change*, *8*(4), 300–304. https://doi.org/10.1038/s41558-018-0105-1

Pérez, F. F., Mercier, H., Vázquez-Rodríguez, M., Lherminier, P., Velo, A., Pardo, P. C., et al. (2013). Atlantic Ocean CO_2 uptake reduced by weakening of the meridional overturning circulation. *Nature Geoscience*, *6*(2), 146–152. https://doi.org/10.1038/ngeo1680

Petit, T., Lozier, M. S., Josey, S. A., & Cunningham, S. A. (2020). Atlantic deep water formation occurs primarily in the Iceland Basin and Irminger Sea by local buoyancy forcing. *Geophysical Research Letters*, *47*(22), 1–9. https://doi.org/10.1029/2020GL091028

Pickart, R. S., Straneo, F., & Moore, G. W. (2003). Is Labrador Sea Water formed in the Irminger basin? *Deep-Sea Research Part I Oceanographic Research Papers*, *50*(1), 23–52. https://doi.org/10.1016/S0967-0637(02)00134-6

Piron, A., Thierry, V., Mercier, H., & Caniaux, G. (2016). Argo float observations of basin-scale deep convection in the Irminger Sea during winter 2011–2012. *Deep-Sea Research Part I Oceanographic Research Papers*, *109*, 76–90. https://doi.org/10.1016/j.dsr.2015.12.012

Sampe, T., & Xie, S. P. (2007). Mapping high sea winds from space: A global climatology. *Bulletin of the American Meteorological Society*, *88*(12), 1965–1978. https://doi.org/10.1175/BAMS-88-12-1965

Slater, T., Shepherd, A., McMillan, M., Leeson, A., Gilbert, L., Muir, A., et al. (2021). Increased variability in Greenland Ice Sheet runoff from satellite observations. *Nature Communications*, *12*(1), 6069. https://doi.org/10.1038/s41467-021-26229-4

Somot, S., Houpert, L., Sevault, F., Testor, P., Bosse, A., Taupier-Letage, I., et al. (2018). Characterizing, modelling and understanding the climate variability of the deep water formation in the North-Western Mediterranean Sea. *Climate Dynamics*, *51*(3), 1179–1210. https://doi.org/10.1007/s00382-016-3295-0

Straneo, F. (2006a). Heat and freshwater transport through the central Labrador Sea. *Journal of Physical Oceanography*, *36*(4), 606–628. https://doi.org/10.1175/JPO2875.1

Straneo, F. (2006b). On the connection between dense water formation, overturning, and poleward heat transport in a convective basin. *Journal of Physical Oceanography*, *36*(9), 1822–1840. https://doi.org/10.1175/JPO2932.1

Våge, K., Pickart, R. S., Sarafanov, A., Knutsen, Ø., Mercier, H., Lherminier, P., et al. (2011). The Irminger Gyre: Circulation, convection, and interannual variability. *Deep-Sea Research Part I Oceanographic Research Papers*, *58*(5), 590–614. https://doi.org/10.1016/j.dsr.2011.03.001

Volkov, D. L. (2005). Interannual variability of the altimetry-derived eddy field and surface circulation in the extratropical North Atlantic Ocean in 1993-2001. *Journal of Physical Oceanography*, *35*(4), 405–426. https://doi.org/10.1175/JPO2683.1

Yashayaev, I., & Loder, J. W. (2017). Further intensification of deep convection in the Labrador Sea in 2016. *Geophysical Research Letters*, *44*(3), 1429–1438. https://doi.org/10.1002/2016GL071668